ISSN: 2640-4133

Research article

Advances in Bioengineering & Biomedical Science Research

Finite Element Analysis of Proximal Femoral Nail Anti-Rotation Blade Combined with Cerclage Wire Fixation for Osteoporotic Subtrochanteric Fracture

Xiaobo Guo[1*], Yu Qiao[2], Xiaonan Liang[2], Jiangtao Jin[1], Jinwei Chen[1], Junyang Liu[1]

[1]*Department of Orthopedic Surgery, Jincheng General Hospital*

[2]*Department of Trauma Orthopedic and Hand Surgery, the First Affliated Hospital of Guangxi Medical University*

[*]Corresponding author

Xiaobo Guo, Jincheng General Hospital, ChangAn Road, JinCheng City, ShanXi Province, China

Submitted: 09 Sep 2021; **Accepted:** 14 Sep 2021; **Published:** 21 Sep 2021

Citation: *Xiaobo Guo, Yu Qiao, Xiaonan Liang, Jiangtao Jin, Jinwei Chen, Junyang Liu (2021) Finite Element Analysis of Proximal Femoral Nail Anti-Rotation Blade Combined with Cerclage Wire Fixation for Osteoporotic Subtrochanteric Fracture. Adv Bioeng Biomed Sci Res 4(3): 78-84.*

Introduction

Osteoporosis is a type of systemic bone disease wherein the patient is highly vulnerable to bone fracture because of the decrease in bone density and quality, destruction of the bone microstructure, and an increase in the bone fragility. Most of the osteoporotic subtrochanteric fractures are unstable in nature, requiring the conservative treatment of a long-duration bed rest and traction; this condition is prone to complications resultant from extended bed rest, often leading to death. Presently, the preferred treatment is internal fixation, such as sliding hip screws, blade plates, locking compression plates, and femoral intramedullary nails [1-8]. Owing to its valuable biological properties, intramedullary nail can be used for the optimal fixation of subtrochanteric fractures [9-11]. Unless any contraindication exist, immediate tolerable weight-bearing activities may be allowed to patients with subtrochanteric femur fractures who have been treated with statically locked intramedullary nails [12]. Considering that the proximal femoral fracture occurs under the traction of the surrounding muscles, it is extremely challenging to perform precision reduction and fixation in the surgery. Inappropriate reduction and selection of internal fixation can easily lead to failure of internal fixation, resulting in complications such as lower limb shortening deformity, hip varus deformity, and nonunion of fracture. Presently, good outcomes have been reported with the use of PFNA combined with cerclage wire for the treatment of subtrochanteric fracture of the femur [13-15]. There are few studies to help decide whether PFNA should be combined with cerclage wire or used alone according the Seinsheimer classification of subtrochanteric fractures.

Compared with the conventional biomechanical analyses, finite element analysis offers the characteristics of various loading modes, multiple test indexes, intuitive experimental results, low research cost, short test cycle, and application in dynamic analysis. In the recent years, the finite element method has been widely applied in the medical field, especially in the field of traumatic orthopedics. In addition, it has been widely used for the optimization and designing of hip prosthesis to assess the risk of femoral neck fracture as well as for the prognosis evaluation of internal fixation treatment [16-18].

In this study, we employed the finite element method to evaluate the stability and necessity of fixation by PFNA in combination with cerclage wire with reference to the Seinsheimer Classification of femoral subtrochanteric fractures in the osteoporotic subtrochanteric fracture and to comprehend the probability of potential complications.

Materials and methods

Three-Dimensional(3D) Models

The research protocol was in accordance with the Helsinki Declaration and duly approved by the Research Ethics Committee of our institution. Written pre-informed consent was obtained from healthy volunteers for their participation in the study.

A 70-year-old healthy volunteer (height: 170 cm, weight: 63 kg) was scanned by the 64-row Siemens spiral CT in the Jincheng General Hospital. The scanning range was from the iliac to the knee joint. The patient was kept in the supine position, with bilateral toes forward, and the posture was maintained consistently with the standing posture on both the legs. The slice thickness was 1 mm, and the images were stored in the DICOM format.

CT data in the DICOM format were imported to the Mimics Research 20.0 Software (Materialise Belgium). After setting the threshold, generating and editing masks, and filling and smoothing, 3D models of the whole and cancellous of the left femur were generated and stored in the STL format.

Next, the femur data was imported to the Geomagic Studio 2014 Software (Raindrop, USA) to remesh, remove spikes, smoothen, extract surfacing, detect and edit contours, construct patches, and fit the surface. The resultant optimized 3D model of the left femur and cancellous bone was obtained, and the relevant IGS file was exported.

The IGS files of the femur whole and cancellous bone were imported to the SolidWorks 2019 and saved. A new assembly was then created and used in the origin coincidence command to combine the two entities. Next, the part mode was entered and the combination was used to give deletion commands in order to construct the femoral cancellous bone and the cortical bone model. The constructed elements were saved in the SLDPRT file format after reconstruction.

We employed the SolidWorks 2019 (Dassault Systems, USA) software to draw the PFNA-II Asian Internal Fixation System. The commands of stretch, cut, loft, array and fillet were used to reconstruct the PFNA nail, spiral blade, and distal locking screw. The PFNA nail length was 170 mm, and the valgus angle was 5 degrees. The screw blade length was 100 mm, the diameter was 10.5 mm, and the neck stem angle was 125 degrees. The elements were saved as the SLDPRT file after reconstruction.

In the SolidWorks 2019, the left femur and PFNA were assembled according to the standard surgical techniques. We confirmed that the Tip-apex distance was ≤25 mm, the spiral blade was located in the mid-lower portion of the femoral neck, and the main nail was in a 3-point contact with the femoral cortex, albeit it did not penetrate. The elements were saved in the SLDPRT file format after reconstruction.

With reference to the Seinsheimer Classification system of subtrochanteric fractures, the fracture types IIB, IIC, IIIA, IIIB, and IV fractures were constructed. Two types of IIC fractures were constructed according to the relative position of the spiral blade and fracture lines. All types of fractures were placed with cerclage wires based on the fracture conditions. The resultant elements were saved in the SLDPRT file after construction (Photo 1).

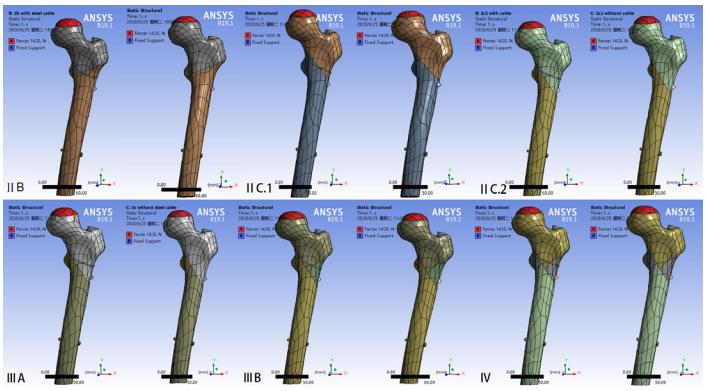

Photo 1: Different models of subtrochanteric fractures according the Seinsheimer classification of subtrochanteric fractures.

Finite Element Analysis of the Model

The assembly of the femur and internal fixation in the SLDPRT format was imported to the ANSYS Workbench 19.1 (ANSYS INC, USA). The mesh command was used to create the mesh, followed by mesh quality check. After meshing, a total of 152455 elements and 246827 nodes were generated in the femoral model. The PFNA model generated 113423 elements and 176018 nodes. The number of elements and nodes generated by other fixed models were slightly different. Convergence tests were performed on all models to verify that element discretization was sufficient for the stress analysis.

The material properties of PFNA internal fixation and the femur were set to isotropy. The property of PFNA internal fixation material was set as titanium alloy (elastic modulus of the osteoporotic cortical bone: 110000 MPa, Poisson's ratio: 0.35) [19-23]. The property of cerclage wire material was set as structural steel. The femoral cortex and cancellous material were set as suggested by previous literature (elastic modulus of osteoporotic cortical bone: 15000 MPa and Poisson's ratio: 0.3, elastic modulus of osteoporosis cancellous bone: 105 MPa and Poisson's ratio: 0.37) [24-28]. The friction coefficient between the bones was set to 0.46, that between the bone and internal fixation was set to 0.3, and that between internal fixation was set to 0.23 [29, 30].

In this study, only the force of the acetabulum on the femoral head was considered. The force was linearly loaded along 10 degrees to the long axis of the femoral shaft and perpendicular to the spherical surface of the femoral head in the anteroposterior view. Past researchers have reported approximately 230% body weight when standing on one leg [31, 32]. The femoral head was loaded with a 1420-N force. Partial resection of the distal femur reduced the amount of computation. the distal end of the model was fixed. Finally, we conducted finite element analysis and assessed the risk of fracture surface sliding, spiral blade cutting-out, the nail and distal lock screw fragmentation on different models.

Results

Model Validation

In order to confirm the validity of the model, a complete femoral model was employed. The material property was assigned to normal cortical and cancellous bone. An axial force of 1500 N was applied to the femoral head. The stress was mainly distributed in the medial-upper portion and the posterolateral-lower portion of the femur, in accordance with the physiological distribution of the human body [33]. The axial stiffness obtained was 0.74 kN/mm, which conforms to that obtained in previous experiments (0.76 ± 0.26 kN/mm) [34].

Total Deformation Distribution

With the accumulation of stress, all fracture models showed lateral fracture gap separation and medial fracture gap compression. The maximum displacement of all fracture models was located at the top of the femoral head (Photo 2). In the models III A, IIIB, and IV, separation occurred between the medial and lateral fracture fragments and the femoral trunk. In the PFNA alone group, the total displacements of the models IIB, IIC.1, IIC.2, IIIA, IIIB, and IV were 1.202, 1.423, 1.582, 1.642, and 1.677 mm, respectively. After the use of PFNA combined with cerclage wire fixation, the total displacements of the models IIB, IIC.1, IIC.2, IIIA, IIIB, and IV were 1.186, 1.311, 1.413, 1.569, 1.446, and 1.948 mm, respectively. After the use of cerclage wire alone, the total displacements of the models IIC.2, IIIB, and IV were reduced by 10.72, 13.74, and 11.89%, respectively (Fig 1).

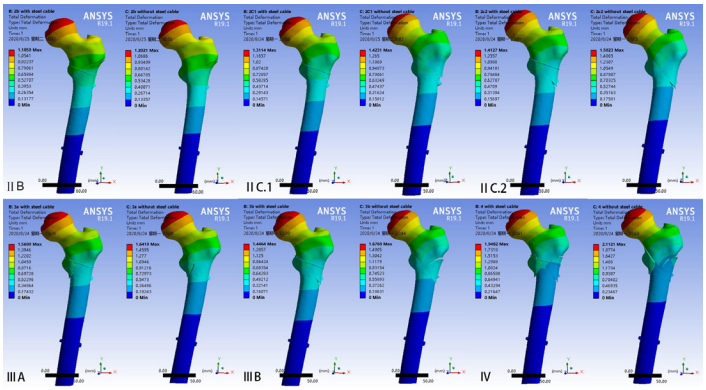

Photo 2: The nephogram of deformation Distribution.

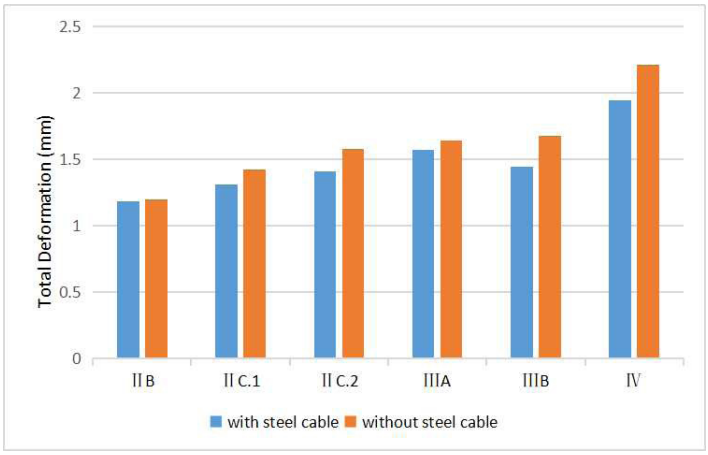

Figure 1: Total deformation distribution between groups.

Sliding Distance of the Fracture Surface

Contact tools were employed to calculate the sliding distance between the two fracture surfaces in order to evaluate the stability of internal fixation. In the PFNA alone group, the maximum sliding distance of the models IIB, IIC.1, IIC.2, IIIA, IIIB, and IV were 0.027, 0.369, 0.385, 0.076, 0.452, and 0.407 mm, respectively. In the group of PFNA combined with cerclage wire fixation, the total displacements of the models IIB, IIC.1, IIC.2, IIIA, IIIB, and IV were 0.019, 0.219, 0.179, 0.065, 0.240, and 0.350 mm, respectively. The sliding distances in the models IIC.1, IIC.2, IIIB, and IV were significantly higher than those in the models IIB and III A. The maximum sliding distance of the model IIC.1 was located on the posteromedial fracture face, which reduced by 40.88% with the use of cerclage wire. The maximum relative displacements in the models IIC.2 and IIIB were located on the medial fracture face, which were reduced by 53.48% and 46.71% with the use of cerclage wire. The maximum sliding distance of the model IV in the anteromedial fracture face was reduced by 14.14% with the use of cerclage wire (Photo 3) (Fig 2).

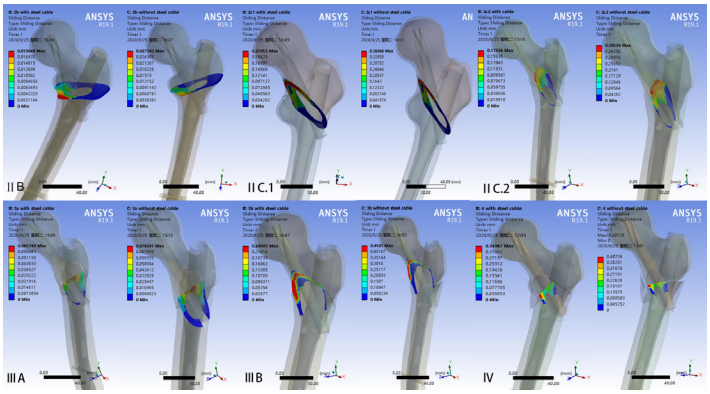

Photo 3: The nephogram of fracture surface sliding.

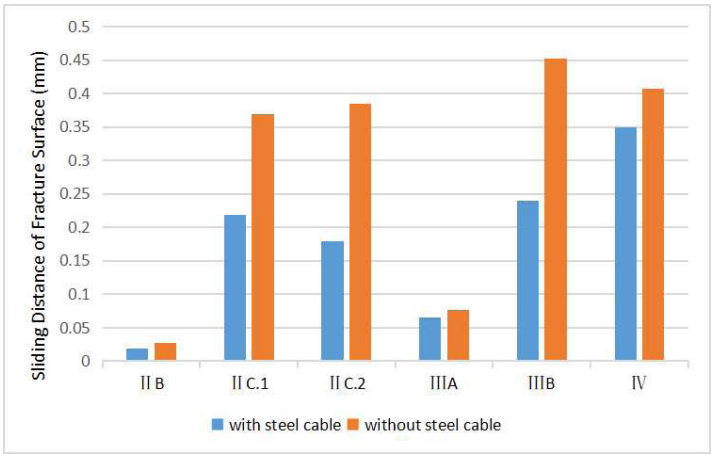

Figure 2: Max fracture surface sliding between groups.

In the PFNA alone group, the maximum equivalent stress for models IIB, IIC.1, IIC.2, IIIA, IIIB, and IV were 4.426, 23.048, 25.236, 8.187, 25.076, and 26.271 MPa, respectively. In the PFNA combined with cerclage wire fixation group, the maximum equivalent stress of the models IIB, IIC.1, IIC.2, IIIA, IIIB, and IV were 4.702, 11.368, 12.855, 10.065, 12.822, and 23.671 MPa, respectively. The stresses of the spiral blade tip in the models IIC.1, IIC.2, IIIB, and IV were significantly higher than those in the models IIB and III A. After using the cerclage wire, the stresses for the models IIC.1, IIC.2, and IIIB significantly decreased by 50.68, 49.06, and 48.87%, respectively (Fig 3).

In the PFNA alone group, the maximum equivalent stress for models IIB, IIC.1, IIC.2, IIIA, IIIB, and IV were 4.426, 23.048, 25.236, 8.187, 25.076, and 26.271 MPa, respectively. In the PFNA combined with cerclage wire fixation group, the maximum equivalent stress of the models IIB, IIC.1, IIC.2, IIIA, IIIB, and IV were 4.702, 11.368, 12.855, 10.065, 12.822, and 23.671 MPa, respectively. The stresses of the spiral blade tip in the models IIC.1, IIC.2, IIIB, and IV were significantly higher than those in the models IIB and III A. After using the cerclage wire, the stresses for the models IIC.1, IIC.2, and IIIB significantly decreased by 50.68, 49.06, and 48.87%, respectively (Fig 3).

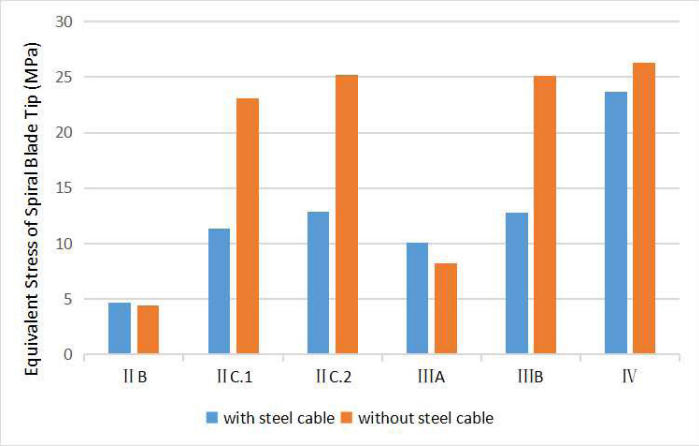

Figure 3: Equivalent Stress of Spiral blade tip between groups.

The Relative Displacement between the Spiral Blade and Femoral Head in Y-axis

In the PFNA alone group, the relative displacements in the models IIB, IIC.1, IIC.2, IIIA, IIIB, and IV were 0.087, 0.224,0.293, 0.167, 0.262, and 0.306 mm, respectively. In the PFNA combined with cerclage wire fixation group, the relative displacement of the models IIB, IIC.1, IIC.2, IIIA, IIIB, and IV were 0.089, 0.170, 0.182, 0.147, 0.189, and 0.274 mm, respectively. The relative displacements of the models IIC.1, IIC.2, IIIB, and IV were significantly higher than those of the models IIB and III A. The relative displacement for the models IIC.1, IIC.2, and IIIB were significantly decreased by 24.11, 37.88, and 27.86%, respectively, in the PFNA combined with cerclage wire group than in the PFNA alone group (Fig 4).

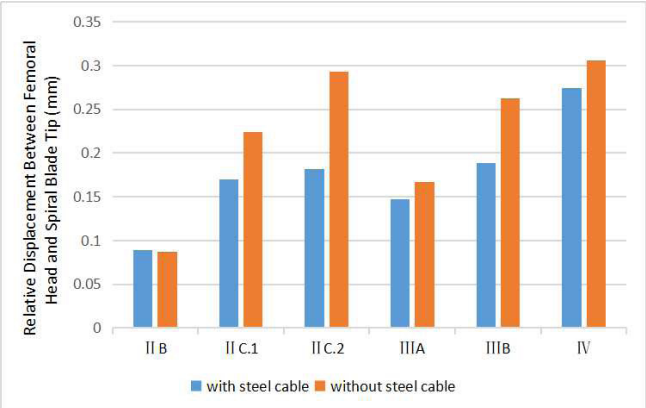

Figure 4: The relative displacement between the spiral blade and femoral head in Y-axis between groups.

Equivalent Stress Distribution of Nails

The equivalent stress distribution area of a nail mainly included the inner and outer portions of the upper-middle region, around the nail-spiral blade interface, and at the distal nail-locking screw interface. The maximum equivalent stress of the model IIb with cerclage wire was distributed across the upper surface of the nail-blade interface. The maximum stress of other models was distributed on the lower surface of the main nail blade interface (Photo 4).

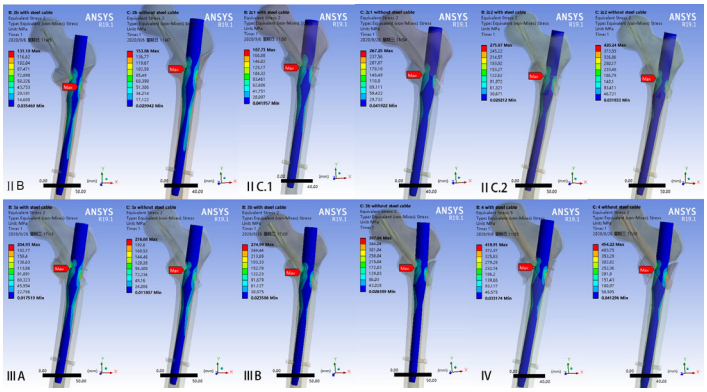

Photo 4: The nephogram of nail stress distribution.

In the PFNA alone group, the maximum equivalent stresses on the models IIB, IIC.1, IIC.2, IIIA, IIIB, and IV were 153.86, 267.25, 420.24, 206.68, 387.04, and 454.22 MPa, respectively. In the PFNA combined with cerclage wire fixation group, the maximum equivalent stresses on the models IIB, IIC.1, IIC.2, IIIA, IIIB, and IV were 131.19, 187.73, 225.87, 204.93, 274.99, and 418.90 MPa, respectively. The maximum equivalent stresses on the models IIC.2, IIIB, and IV were significantly higher than those in the models IIB, IIC.1, and III A. In the PFNA combined with cerclage wire group, the stresses on the models IIC.1, IIC.2, and IIIB were significantly decreased by 29.75, 46.25, and 28.95%, respectively (Fig 5).

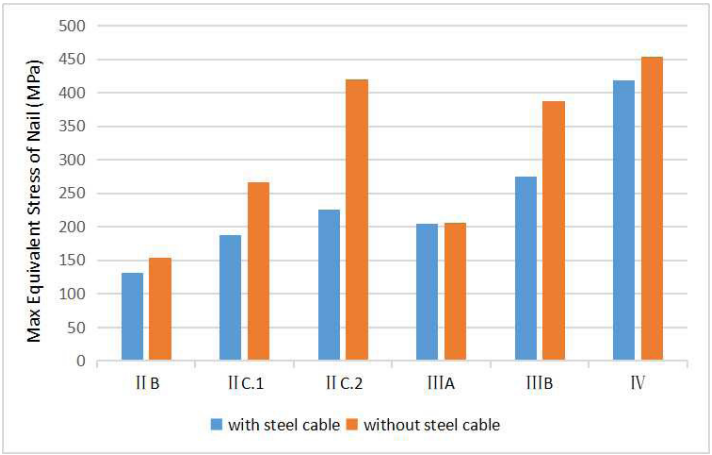

Figure 5: The max equivalent stress distribution of nails between groups.

Equivalent Stress Distribution of the Distal Lock Screw

The maximum equivalent stress was distributed above the nail-distal lock screw interface in the model IIB with cerclage wire, while it was distributed below the nail-distal lock screw interface in the other models (Photo 5).

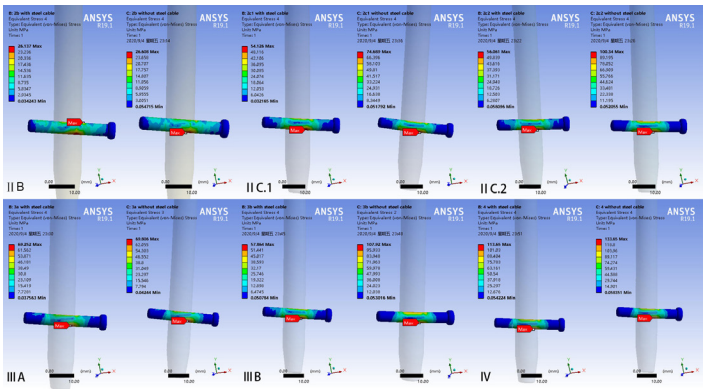

Photo 5: The nephogram of distal lock screw stress distribution.

In the PFNA alone group, the maximum equivalent stresses on the models IIB, IIC.1, IIC.2, IIIA, IIIB, and IV were 26.608, 74.689, 100.34, 69.806, 107.920, and 133.65 MPa, respectively. In the PFNA combined with cerclage wire fixation group, the maximum equivalent stresses on the models IIB, IIC.1, IIC.2, IIIA, IIIB, and IV were 26.173, 54.261, 56.061, 69.252, 57.864, and 113.650 MPa, respectively. The maximum equivalent stresses on the models IIC.1, IIC.2, IIIB, and IV were significantly higher than those in the models IIB and III A. In the combination group, the stresses on models IIC.1, IIC.2, and IIIB significantly decreased by 27.35, 44.13, and 46.38%, respectively, relative to that in the PFNA group (Fig 6).

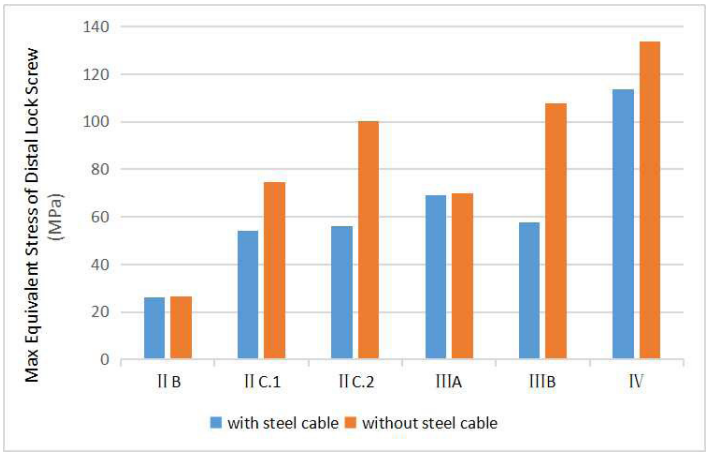

Figure 6: The max equivalent stress distribution of distal lock screw between groups.

Discussion

The fracture within the area 5-cm below the lower boundary of the lesser trochanter is called the subtrochanteric fracture of the femur. Subtrochanteric fractures account for approximately 5-20% of all proximal femoral fractures [35, 36]. Biologically, the subtrochanteric region is the junction of cancellous bone between the trochanter and the cortical bone of the femoral shaft, which is the transition area from a wide to narrow bone marrow cavity, where the distribution of the blood vessels is limited. In the biomechanical terms, the subtrochanteric region of the femur is a high stress concentration area that bears the highest tensile and compressive stresses in the human skeleton [37]. In complex subtrochanteric fracture of the femur, the proximal fragment of the fracture is in the flexion, abduction, and external rotational position owing to the traction of the medial gluteus minimus and the iliopsoas muscles, which usually results in varus deformity and displacement [38]. Strong muscle traction makes anatomic reduction difficult. As a result, implant failure occurs, further resulting in increased nonunion rate of the fracture [7]. Moreover, high compressive and tensile stresses contribute to the development of nonunions [39]. As most of the patients with osteoporotic subtrochanteric fractures are elderly, they cannot tolerate long-term bed rest. Therefore, appropriate postoperative exercise is extremely important. Hence, good fracture stability is undoubtedly the main factor for successful recovery [40].

The main internal fixation methods of subtrochanteric fracture include intramedullary fixation and external fixation. Intramedullary nailing is the main method for intramedullary fixation, while anatomical locking plate is used for external fixation. Intramedullary fixation is superior to extramedullary fixation in the biomechanical terms because central fixation reduces the bending moment, reduces the torsion force, and enhances the anti-rotation stability.

Intramedullary nail has been widely used in elderly patients with osteoporotic intertrochanteric and subtrochanteric fractures. For the intertrochanteric fractures, the intramedullary nail is easy to implant with fewer complications and the convenience of early weight-bearing allowance. The approach involving minimally invasive wire cerclage can support the medial cortex, increase the load tolerance, and avoid the varus displacement of proximal fragments or screw cutting out from the femoral head. Recently, several studies showed that wire cerclage can prevent fracture block displacement while enhancing the stability of intramedullary fixation [41]. As compared with extramedullary fixation,the intramedullary nail approach combined with steel wire cerclage results in lesser trauma and bears stress through the central medullary cavity, while reducing the bending moment, bearing lesser torsion, and showing good anti-rotation stability [36, 42-45].

In this study, we employed the CT data of a 70-year-old healthy volunteer in order to reconstruct the femoral cortex and cancellous bone. The material attribute was set to osteoporotic bone. The load of femoral head simulate the daily load of the hip. We aim to access protective effect of cerclage wire on the internal fixation and fracture stability by finite element analysis.

In this study, we demonstrated that, with an increase in the fracture comminution degree and the stability of fracture surface, the risk of PFNA blade cutting-out and distal locking nail breaking increased correspondingly. In the model IIB, the use of cerclage wire could slightly reduce the risk of sliding of the fracture surface and the spiral blade cutting-out. In the models IIC.1 and IIC.2, the use of cerclage wire could significantly reduce the risk of sliding of the fracture surface, spiral blade cutting-out, and the nail and distal lock screw fragmentation, but the effect was more significant in

the model IIC.2. In the model IIIB, the use of cerclage wire could significantly reduce the risk of sliding at the fracture surface, with the spiral blade cutting-out, and the nail and distal lock screw fragmentation. In the model IV, the use of cerclage wire could slightly reduce the risk of sliding at the fracture surface, the spiral blade cutting-out, and the nail and distal lock screw fragmentation. In the models IIC.1, IIC.2, and IIIB, the use of cerclage wire resulted in a good protective effect on the internal fixation and fracture stability. In the model IIB with cerclage wire, no significant protective effect was noted on the internal fixation and fracture stability. In the models IIIB and IV, the effect of cerclage wire was only to protect the movement of the fracture fragments.

There were some limitations. First, the subtrochanteric fractures examined in this study reflected a simplified model, which ignored the effects of muscles, ligaments, and joint capsules. Second, the hip joint is a multi-axial joint that can perform the actions of flexion and extension, abduction, and rotation. In the future, it will be necessary to conduct hip joint loading and torsion experiments from multiple perspectives. Third, the current model employs CT data of a volunteer, but the length and shape of the femur have individual differences; this issue necessitates the employment of a larger sample size. Fourth, it is necessary to combine the finite element method with cadaver experiments for a more definitive inference of the study reports.

Conclusion

With reference to the Seinsheimer classification, the fractures in this study of subtrochanteric fractures IIC and IIIB, the use of cerclage wire demonstrated a good protective effect on internal fixation and fracture stability. In the models IIIB and IV, the effect of cerclage wire in protecting the movement of fracture fragments was noted.

Declaration of Competing Interest

There was no conflict of interest for this paper.

References

1. Matre K, LI Havelin, JE Gjertsen, Tarjei Vinje, Birgitte Espehaug, et al. (2013) Sliding hip screw versus IM nail in reverse oblique trochanteric and subtrochanteric fractures. A study of 2716 patients in the Norwegian Hip Fracture Register. Injury 44: 735-742.
2. Ploeger MM, M Gathen, C Struwe, Richard Placzek (2019) Proximal Femoral Osteotomies in the Adolescence: Indications and Treatment Strategies. Z Orthop Unfall 159:153-163.
3. Kumar N, H Kataria, C Yadav, Bharath S Gadagoli, Rishi Raj (2014) Evaluation of proximal femoral locking plate in unstable extracapsular proximal femoral fractures: Surgical technique & mid term follow up results. J Clin Orthop Trauma 5: 137-145.
4. Latifi MH, K Ganthel, S Rukmanikanthan, Azura Mansor, Tunku Kamarul, et al. (2012) Prospects of implant with locking plate in fixation of subtrochanteric fracture: experimental demonstration of its potential benefits on synthetic femur model with supportive hierarchical nonlinear hyperelastic finite element analysis. Biomed Eng Online 11: 23.
5. Yoo MC, YJ Cho, KI Kim, Mohamad Khairuddin, Young Soo Chun (2005) Treatment of unstable peritrochanteric femoral fractures using a 95 degrees angled blade plate. J Orthop Trauma 19: 687-692.
6. Karahan G, K Yamak, T Kocoglu, Taskin Altay, Cemil Kayali (2020) The effect of implant choice on varus angulation and clinical results in the management of subtrochanteric fractures. J Orthop 20: 46-49.
7. Jang JH, JM Ahn, HJ Lee, Nam Hoon Moon (2017) Surgical Outcomes of Biologic Fixation for Subtrochanteric Fracture Using Locking Compression Plates. Hip Pelvis 29: 68-76.
8. Vaishya R, AK Agarwal, N Gupta, Vipul Vijay (2016) Reversed distal femoral locking plate for failed proximal femoral nail with non-union of proximal femoral fractures. Int Orthop 40: 1709-1715.
9. Forward DP, CJ Doro, RV O'Toole, Hyunchul Kim, John C P Floyd, et al. (2012) A biomechanical comparison of a locking plate, a nail, and a 95 degrees angled blade plate for fixation of subtrochanteric femoral fractures. J Orthop Trauma 26: 334-340.
10. Rahme DM, IA Harris (2007) Intramedullary nailing versus fixed angle blade plating for subtrochanteric femoral fractures: a prospective randomised controlled trial. J Orthop Surg (Hong Kong) 15: 278-281.
11. Kwang Kyoun Kim, Yougun Won, Danica H Smith, Gi Soo Lee, Hee Young Lee (2017) Clinical Results of Complex Subtrochanteric Femoral Fractures with Long Cephalomedullary Hip Nail. Hip Pelvis 29: 113-119.
12. Cunningham BP, A Ali, HR Parikh, Austin Heare, Breanna Blaschke, et al. (2020) Immediate weight bearing as tolerated (WBAT) correlates with a decreased length of stay post intramedullary fixation for subtrochanteric fractures: a multicenter retrospective cohort study. Eur J Orthop Surg Traumatol 31: 235-243.
13. Schopper C, M Faschingbauer, RT Moeller, F Gebhard, L Duerselen, et al. (2020) Modified Candy-Package technique vs Cerclage technique for refixation of the lesser trochanteric fragment in pertrochanteric femoral fractures. A biomechanical comparison of 10 specimens. Injury 51: 1763-1768.
14. Kilinc BE, Y Oc, A Kara, Ramazan Erden Erturer (2018) The effect of the cerclage wire in the treatment of subtrochanteric femur fracture with the long proximal femoral nail: A review of 52 cases. Int J Surg 56: 250-255.
15. Codesido P, A Mejia, J Riego, Cristina Ojeda Thies (2017) Cerclage Wiring Through a Mini-Open Approach to Assist Reduction of Subtrochanteric Fractures Treated With Cephalomedullary Fixation: Surgical Technique. J Orthop Trauma 31: 263-268.
16. Fleps I, WS Enns Bray, P Guy, Stephen J Ferguson, Peter A Cripton, et al. (2018) On the internal reaction forces, energy absorption, and fracture in the hip during simulated sideways fall impact. PLoS One 13: 0200952.
17. Yang L, N Peel, JA Clowes, Eugene V McCloskey, Richard Eastell (2009) Use of DXA-based structural engineering models of the proximal femur to discriminate hip fracture. J Bone Miner Res 24: 33-42.
18. Wang Y, JX Ma, T Yin, Zhe Han, Shuang Shuang Cui, et al. (2019) Correlation Between Reduction Quality of Femoral Neck Fracture and Femoral Head Necrosis Based on Biomechanics. Orthop Surg 11: 318-324.
19. Hinuber C, C Kleemann, RJ Friederichs, L Haubold, H J

Scheibe, et al. (2010) Biocompatibility and mechanical properties of diamond-like coatings on cobalt-chromium-molybdenum steel and titanium-aluminum-vanadium biomedical alloys. J Biomed Mater Res A 95: 388-400.
20. Shibo G, Q Xuanhui, H Xinbo, ZhouTing, DuanBohu (2006) Powder injection molding of Ti–6Al–4V alloy. Journal of Materials Processing Technology 173: 310-314.
21. Goffin J, P Pankaj, A Simpson, R Seil, TG Gerich (2013) Does bone compaction around the helical blade of a proximal femoral nail anti-rotation (PFNA) decrease the risk of cut-out? A subject-specific computational study. Bone & joint research 2: 79-83.
22. Carney K, JM Pereira, D Revilock, P Matheny (2009) Jet engine fan blade containment using an alternate geometry. International journal of impact engineering 36: 720-728.
23. Helgason B, M Viceconti, TP Rúnarsson, Sigurour Brynjólfsson (2008) On the mechanical stability of porous coated press fit titanium implants: a finite element study of a pushout test. Journal of biomechanics 41: 1675-1681.
24. Yeni YN, CU Brown, TL Norman (1998) Influence of bone composition and apparent density on fracture toughness of the human femur and tibia. Bone 22: 79-84.
25. McCalden RW, JA McGeough, MB Barker, CM Court Brown (1993) Age-related changes in the tensile properties of cortical bone. The relative importance of changes in porosity, mineralization, and microstructure. J Bone Joint Surg Am 75: 1193-1205.
26. Dong XN, XE Guo (2004) The dependence of transversely isotropic elasticity of human femoral cortical bone on porosity. J Biomech 37: 1281-1287.
27. Ma Z, J Chen, F Lan (2014) Biomechanical response and injury of occupant's pelvis in side impacts: effects of the femoral head and loading conditions. Journal of Mechanics in Medicine and Biology 14: 1440001.
28. Kawabata Y, K Matsuo, Y Nezu, Takayuki Kamiishi, Yutaka Inaba, et al. (2017) The risk assessment of pathological fracture in the proximal femur using a CT-based finite element method. Journal of Orthopaedic Science 22: 931-937.
29. Eberle S, C Gerber, G von Oldenburg, Sven Hungerer, Peter Augat (2009) Type of hip fracture determines load share in intramedullary osteosynthesis. Clin Orthop Relat Res 467: 1972-1980.
30. Nuno N, M Amabili, R Groppetti, A Rossi (2002) Static coefficient of friction between Ti-6Al-4V and PMMA for cemented hip and knee implants. J Biomed Mater Res 59: 191-200.
31. Konrath GA, AJ Hamel, SA Olson, B Bay, N A Sharkey (1998) The role of the acetabular labrum and the transverse acetabular ligament in load transmission in the hip JBJS 80: 1781.
32. Bergmann G, G Deuretzbacher, M Heller, F Graichen, A Rohlmann, et al. (2001) Hip contact forces and gait patterns from routine activities. J Biomech 34: 859-871.
33. Levadnyi I, J Awrejcewicz, Y Zhang, Yaodong Gu (2020) Comparison of femur strain under different loading scenarios: Experimental testing. Proc Inst Mech Eng H 235:17-27.
34. Papini M, R Zdero, EH Schemitsch (2007) The biomechanics of human femurs in axial and torsional loading: comparison of finite element analysis, human cadaveric femurs, and synthetic femurs. J Biomech Eng 129: 12-19.
35. Ekstrom W, G Nemeth, E Samnegard, Nils Dalen, Jan Tidermark (2009) Quality of life after a subtrochanteric fracture: a prospective cohort study on 87 elderly patients. Injury 40: 371-376.
36. Codesido P, A Mejia, J Riego, Cristina Ojeda Thies (2017) Subtrochanteric fractures in elderly people treated with intramedullary fixation: quality of life and complications following open reduction and cerclage wiring versus closed reduction. Arch Orthop Trauma Surg 137: 1077-1085.
37. Barquet A, G Mayora, J Fregeiro (2004) The treatment of subtrochanteric nonunions with the long gamma nail: twenty-six patients with a minimum 2-year follow-up. J Orthop Trauma 18: 346-353.
38. Lundy DW (2007) Subtrochanteric femoral fractures. J Am Acad Orthop Surg 15: 663-671.
39. Pugh KJ, RA Morgan, JT Gorczyca, D Pienkowski (1998) A mechanical comparison of subtrochanteric femur fracture fixation. J Orthop Trauma 12: 324-329.
40. Canadian Orthopaedic Trauma S (2003) Nonunion following intramedullary nailing of the femur with and without reaming. Results of a multicenter randomized clinical trial. J Bone Joint Surg Am 85: 2093-2096.
41. Lv C, Y Fang, L Liu, Guanglin Wang, Tianfu Yang, et al. (2011) The new proximal femoral nail antirotation-Asia: early results. Orthopedics 34: 351.
42. Mukherjee P, JE Brattgjerd, S Niratisairak, Jan Rune Nilssen, Knut Strømsøe, et al. (2019) The stabilising effect by a novel cable cerclage configuration in long cephalomedullary nailing of subtrochanteric fractures with a posteromedial wedge. Clin Biomech (Bristol, Avon) 68: 1-7.
43. Mehta NJ, T Goldsmith, A Lacey, Gautam Reddy, Veenesh Selvaratnam, et al. (2019) Outcomes of Intramedullary Nailing with Cerclage Wiring in Subtrochanteric Femoral Fractures. Strategies Trauma Limb Reconstr 14: 29-33.
44. Karayiannis P, A James (2019) The impact of cerclage cabling on unstable intertrochanteric and subtrochanteric femoral fractures: a retrospective review of 465 patients. Eur J Trauma Emerg Surg 46: 969-975.
45. Trikha V, S Das, P Agrawal, Arkesh M, Sunil Kumar Dhaka (2018) Role of percutaneous cerclage wire in the management of subtrochanteric fractures treated with intramedullary nails. Chin J Traumatol 21: 42-49.